



**HAL**  
open science

**Discussion on ‘Palaeoseismic structures in Quaternary sediments, related to an assumed fault zone north of the Permian Peissen-Gnutz salt structure (NW Germany) – Neotectonic activity and earthquakes from the Saalian to the Holocene’ (Grube, 2019)**

Pascal Bertran, Kevin Manchuel, Deborah Sicilia

► **To cite this version:**

Pascal Bertran, Kevin Manchuel, Deborah Sicilia. Discussion on ‘Palaeoseismic structures in Quaternary sediments, related to an assumed fault zone north of the Permian Peissen-Gnutz salt structure (NW Germany) – Neotectonic activity and earthquakes from the Saalian to the Holocene’ (Grube, 2019). *Geomorphology*, 2020, 365, pp.106704. 10.1016/j.geomorph.2019.03.010 . hal-03136518

**HAL Id: hal-03136518**

**<https://hal.science/hal-03136518>**

Submitted on 9 Feb 2021

**HAL** is a multi-disciplinary open access archive for the deposit and dissemination of scientific research documents, whether they are published or not. The documents may come from teaching and research institutions in France or abroad, or from public or private research centers.

L’archive ouverte pluridisciplinaire **HAL**, est destinée au dépôt et à la diffusion de documents scientifiques de niveau recherche, publiés ou non, émanant des établissements d’enseignement et de recherche français ou étrangers, des laboratoires publics ou privés.

Manuscript Number: GEOMOR-8414R1

Title: Discussion on 'Palaeoseismic structures in Quaternary sediments, related to an assumed fault zone north of the Permian Peissen-Gnutz salt structure (NW Germany) - Neotectonic activity and earthquakes from the Saalian to the Holocene' (Grube, 2019)

Article Type: Reply

Keywords: Palaeoseismology; Permafrost; Brittle deformation

Corresponding Author: Dr. Pascal Bertran, PhD

Corresponding Author's Institution: INRAP / PACEA

First Author: Pascal Bertran, PhD

Order of Authors: Pascal Bertran, PhD; Kevin Manchuel, Ph.D.; Deborah Sicilia, Ph.D.

Abstract: We discuss the significance of deformation structures in Quaternary sediments observed by Grube (2019) in the Peissen quarries (NW Germany) in light of the geological context. Evidence for polygonal patterns visible in aerial images in the study area shows that the wedge structures interpreted by Grube (2019) as earthquake-induced sand blows may rather correspond to thermal contraction cracks filled with aeolian sand in a permafrost environment. In the study sites, brittle deformations caused by (i) the rise of a salt diapir, (ii) salt dissolution, (iii) the development of Pleistocene permafrost and (iv) possibly, water circulation under pressure in the Scandinavian ice sheet margin may have coexisted. We support the idea that, while the morphology of deformation generally makes it possible to determine the stress state to which the sediments have been subjected and the quantity of water available in the system at the time of deformation, the nature of the factors causing the stresses remains difficult to identify. In the end, we highlight other useful criteria that should be privileged for palaeoseismic research in such complex geological settings.

1 Discussion on 'Palaeoseismic structures in Quaternary sediments, related to an assumed  
2 fault zone north of the Permian Peissen-Gnutz salt structure (NW Germany) – Neotectonic  
3 activity and earthquakes from the Saalian to the Holocene' (Grube, 2019)

4

5 Pascal Bertran<sup>1\*</sup>, Kevin Manchuel<sup>2</sup>, Deborah Sicilia<sup>2</sup>

6 <sup>1</sup> Inrap / PACEA, bâtiment B2, allée Geoffroy-Saint-Hilaire, 33615 Pessac, France

7 <sup>2</sup> EDF, TEGG/Service Géologique Géotechnique, 905 Avenue du Camp de Menthe, 13097 Aix-en-  
8 Provence, France

9 \* Corresponding author. Email address: [pascal.bertran@inrap.fr](mailto:pascal.bertran@inrap.fr)

10

## 11 Abstract

12 We discuss the significance of deformation structures in Quaternary sediments observed by Grube  
13 (2019) in the Peissen quarries (NW Germany) in light of the geological context. Evidence for  
14 polygonal patterns visible in aerial images in the study area shows that the wedge structures  
15 interpreted by Grube (2019) as earthquake-induced sand blows may rather correspond to thermal  
16 contraction cracks filled with aeolian sand in a permafrost environment. In the study sites, brittle  
17 deformations caused by (i) the rise of a salt diapir, (ii) salt dissolution, (iii) the development of  
18 Pleistocene permafrost and (iv) possibly, water circulation under pressure in the Scandinavian ice  
19 sheet margin may have coexisted. We support the idea that, while the morphology of deformation  
20 generally makes it possible to determine the stress state to which the sediments have been  
21 subjected and the quantity of water available in the system at the time of deformation, the nature of  
22 the factors causing the stresses remains difficult to identify. In the end, we highlight other useful  
23 criteria that should be privileged for palaeoseismic research in such complex geological settings.

24 Keywords: Palaeoseismology; Permafrost; Brittle deformation

25

## 26 1. Introduction

27 Grube's (2019) article on brittle and ductile deformations affecting Quaternary sediments in the  
28 Peissen region (northwest Germany) provides interesting data on potential traces of  
29 palaeoearthquakes and is part of a recent effort to extend seismicity catalogues in Europe beyond  
30 the period for which instrumental data and historical texts are available. These deformation

31 structures complement the many other structures already described in northern Europe, particularly  
32 by [Hoffmann and Reicherter \(2012\)](#), [Brandes and Winsemann \(2013\)](#), [van Loon and Pisarska-Jamroz](#)  
33 [\(2014\)](#) and [van Loon et al. \(2016\)](#), which were also interpreted as earthquake-induced. However, the  
34 geographical proximity of all these structures does not constitute proof of a common origin. The  
35 main reasons for this relate to the complex local geomorphological context, marked by (1) the  
36 development of permafrost during the last glaciation, (2) the proximity of the Scandinavian ice sheet  
37 during the last Glacial Maximum, and (3) the presence of a salt diapir in the immediate vicinity of the  
38 study sites. These aspects will be developed in detail here. The outcome of this analysis is that, while  
39 the morphology of deformation generally makes it possible to determine the stress state to which  
40 the sediments have been subjected and the quantity of water available in the system at the time of  
41 deformation, the nature of the factors causing the stresses remains difficult to identify. Laboratory  
42 experiments and field observations indicate that similar brittle and/or ductile deformations may  
43 occur in relation to various geomorphological processes. Therefore, the multiplicity of potential  
44 factors that may have been involved in the sector studied by [Grube \(2019\)](#) does not make it possible  
45 to determine confidently the origin of the deformation structures.

46

## 47 2. Sand blows and sand wedges in a permafrost context

48 The wedge-shaped structures filled with sand described by [Grube \(2019\)](#) and interpreted as sand  
49 blows due to ground fluidization caused by seismic shaking are very similar to the wedges caused by  
50 thermal contraction of the ground in periglacial environments and filled with aeolian sand (sand  
51 wedges) or a mixture of sand and ice (composite wedge pseudomorphs) (e.g., [Murton, 2013](#);  
52 [Andrieux et al., 2016a, b](#)). These wedges have a V shape, sand veins extending from the base  
53 (apophyses), a depth (up to 1.7 m) and an internal organization typical of periglacial structures.  
54 Vertical lamination is preserved in one of the wedges illustrated in Fig. 11e of [Grube \(2019\)](#). The  
55 lamination, common in thermal contraction wedges, is related to repeated cracking of the ground  
56 during winters and the infiltration of aeolian sand into the crack ([Fig. 1](#)). When the filling is composed  
57 of sand and ice (composite wedges), melting of ice causes the lamination to vanish and the wedge to  
58 deform. Coarser material from the host sediment can fill the depression. [Ghysels and Heyse \(2006\)](#)  
59 and [Buylaert et al \(2009\)](#) have described similar examples in Belgium OSL-dated to the Weichselien  
60 and Saalien. Creep of fine-grained host material during melting or repeated thaw cycles can also lead  
61 to the formation of globular structures comparable to those shown in [Grube's \(2019\) Fig. 11b](#) ([Fig.](#)  
62 [1D](#)).

63 One of the most relevant criteria for discriminating these structures from sand blows is their  
64 organization into large polygons, which reach 10 to 30 m in diameter. Unfortunately, [Grube \(2019\)](#)

65 has not documented this aspect. However, some data indicate that the presence of sand wedges or  
66 composite wedge pseudomorphs is highly probable in the study area. These data are (1) polygons  
67 visible on satellite photographs accessible in Google Earth; one of the identified sites is located in the  
68 immediate vicinity of Pit 3, another of Pit 2 (Fig. 2); (2) the mention by Christensen (1978) of  
69 abundant fossil thermal contraction polygons visible in aerial photographs in Denmark and northern  
70 Germany; the geo-referencing of Christensen's map shows that the study sites are located in an area  
71 where more than 5% of agricultural land is affected by polygons; and (3) the concomitance of  
72 continuous permafrost during the last glaciation (Vandenberghe et al., 2014) and coversand  
73 deposition (Kasse, 1997; Zeeberg, 1998), which is a pattern highly favourable to the formation of  
74 sand wedges over large surfaces. Therefore, the interpretation of these structures as periglacial sand  
75 wedges rather than seismogenic sand blows seems most likely in the current state of the analysis and  
76 a seismic origin cannot therefore be retained without more supporting evidence.

### 77 3. Brittle deformation

78 Unconsolidated and well-drained sediments under stress deform in a brittle manner. The stress can  
79 be caused by wide range of geological processes. Many experiments using analog models under  
80 stress have been described in the literature. These models use cohesionless granular materials, most  
81 often sand, sometimes interlayered with ductile levels (cohesive wet clays, or purely viscous silicone  
82 paste). The results constitute a data set that can be used to understand the brittle deformation of  
83 non-lithified Quaternary sediments.

84 Experiments by Komuro (1987) and Walter and Troll (2001) reproduced the growth of a lenticular  
85 body (a putty ball or an inflated chamber) under a granular cover. The increase in volume leads to  
86 the formation of a dome and the development of subvertical radial cracks at the top (Fig. 3A,B). As  
87 the dome grows, cracks are formed that cut at right angles the radial cracks and are arranged in a  
88 more or less concentric pattern. At the top of the dome, the blocks bounded by the cracks collapse,  
89 leading to the formation of a polygonal central depression limited by normal faults. Walter and Troll  
90 (2001) reproduced the succession of growth phases followed by collapse of the cover. The  
91 interaction between the fractures created during swelling and those related to collapse generates  
92 blocks of variable size and a high degree of material fragmentation (Fig. 3F).

93 This type of structure accurately reflects the fracturing of the sediment or peat layer that covers  
94 intrusive ice mounds (pingos, frost blisters) or segregated ice mounds (lithalsas) in a periglacial  
95 context. Examples have been described in the Canadian Arctic by Mackay (1988, 1998) and Pollard  
96 (1991) (Fig. 4A). Davison et al. (2000) and Marco et al. (2002) also observed a system of radial and  
97 tangential cracks in the sedimentary cover at the periphery of salt diapirs (Fig. 4B). In the example

98 detailed by [Marco et al. \(2002\)](#), many structures correspond to clastic dykes and probably result from  
99 the filling of cracks opened from the surface, which were formed in connection with the rise of the  
100 diapir.

101 Experiments that reproduce the rise of a block of substratum, and those that simulate the collapse of  
102 an unconsolidated cover over a cavity, provide comparable results. In both cases, the faults are  
103 concentrated to a limited area at the edge of the raised block or the cavity. [Sanford's \(1959\)](#)  
104 experiments consisted in lifting a rigid block limited by vertical edges under a cover of sand or sand  
105 and clay. Reverse curved faults propagate towards the surface and the subsided area ([Fig. 3C](#)). As  
106 pointed out by [Sanford \(1959\)](#), the reverse faults, which are subvertical at the base and evolve into  
107 thrusts towards the surface, are not related to horizontal compression in the model, but to vertical  
108 movements at depth. Similar results were also obtained in a series of experiments designed to  
109 reproduce the roof collapse over a cavity ([Roche et al., 2001; Walter and Troll, 2001; Geyer et al.,](#)  
110 [2006; Coumans and Stix, 2016](#)). In these experiments, bell-shaped reverse fractures form above the  
111 cavity together with annular extension fractures starting from the surface at the periphery.  
112 Progressive roof collapse occurs in connection with the propagation of the bell-shaped fractures up  
113 to the surface ([Fig. 3D,E](#)). [Coumans and Stix \(2016\)](#) reproduced the situation in which the thickness of  
114 the cover is not homogeneous. In this case, subsidence associated with reverse faulting occurs where  
115 the sediment thickness above the cavity is lowest, whereas normal faults develops at the opposite  
116 side ([Fig. 3G](#)). The final depression has an asymmetrical shape.

117 Many examples of curved reverse faults and associated normal faults have been described in natural  
118 environments. They comprise the cover of salt diapirs undergoing dissolution ([Simon and Soriano,](#)  
119 [1986; Davison et al., 1996](#)) ([Fig. 4B](#)), sediments affected by the collapse of a karstic cavity ([Soriano et](#)  
120 [al., 2012; Simon et al., 2014; Luzón et al., 2012](#)) ([Fig. 4E](#)), subglacial deposits (eskers) deformed by  
121 glacier melt-out ([McDonald and Shilts, 1975](#)), and lahars or fluvio-glacial deposits (jökulhlaup)  
122 deformed by melting of ice-blocks ([Branney and Gilbert, 1995; Fay, 2000](#)). [Calmels et al. \(2008\)](#)  
123 identified reverse ice-filled faults dipping 50 to 90° in a segregated ice mound (lithalsa) in northern  
124 Quebec. According to [Calmels et al. \(2008\)](#), these faults formed during the growth of ice lenses  
125 during permafrost build-up. Reverse faults have also been identified in ramparts created by the  
126 melting of Pleistocene ice mounds ([Payette and Séguin, 1979; Kasse and Bohncke, 1992; Pissart,](#)  
127 [2000; Bertran et al., 2018](#)) and in thermokarst lake deposits ([Murton, 1996; Bertran et al., 2018](#)) ([Fig.](#)  
128 [4C](#)).

129 Other experiments have reproduced deformations created by shortening ([Bonini et al., 2000; Bonini,](#)  
130 [2007](#)). In these models, detachment occurs at the substratum - cover interface and reverse faults

131 with low dip (thrusts) form in the cover to accommodate the shortening (Fig. 3E). Thrusting leads to  
132 the formation of an anticline at the top of the ramp and conjugate reverse faults delimiting pop-up  
133 structures develop. The frontal bulge can collapse along normal faults that form as shortening and  
134 bulging progress.

135 This type of deformation is typically observed in the frontal bulge of landslides (Coombs and Norris,  
136 1981; McCalpin and Thakkar, 2003) (Fig. 4D) and at the front of emerging deep-seated reverse faults  
137 (Philip et al., 1992; McCalpin and Thakkar, 2003).

138 In summary, the available models show that it is possible to identify the stress state that caused  
139 brittle deformation from the fracture geometry. However, the factors underlying stress remain more  
140 difficult to determine and observations in natural environments indicate that many geological  
141 processes are able to generate similar deformations. Comparable conclusions were also drawn for  
142 soft-sediment deformations (e.g., Moretti et al., 2016). Analysis of the fracture pattern can provide  
143 insight into the factors that may be involved. However, the usually limited extent (i.e., a few tens of  
144 metres) of the outcrops is one of the main limitations for documenting accurately the general  
145 fracture pattern. An exception is fracturing due to thermal contraction of the ground in a periglacial  
146 context, where the growth of ice or sand wedges generates easily identifiable polygonal patterns.

147 The site studied by Grube (2019) is located in a complex geological environment, where  
148 deformations created by the rise of a salt diapir, salt dissolution, the development of Pleistocene  
149 permafrost and possibly, by water circulation under pressure in the Scandinavian ice sheet margin  
150 (see Boulton et al., 1993; Murton, 2005; Ravier et al., 2015) have overlapped. Consequently, this site  
151 seems unfavourable to the detection of palaeoearthquakes, insofar as the structures observed at the  
152 scale of the outcrops do not allow the factors potentially involved to be discriminated against. The  
153 association of normal and reverse faults (Fig. 12 of Grube (2019)) may well reflect the deformation  
154 associated with the rise and dissolution of the underlying salt diapir, or that created by the growth  
155 and melting of ice bodies during the Weichselian, rather than earthquake-induced processes. Diapir  
156 uplift caused by loading of the surrounding land by the Weichselian ice sheet likely occurred as  
157 demonstrated by Lang et al. (2014).

#### 158 4. Conclusion and prospects

159 The arguments proposed by Grube (2019) for a seismic origin of the structures observed in the  
160 Peissen quarries are not convincing when considering the context. In such geological settings, the  
161 types of criteria that should be favoured in palaeoseismic research are (1) surface lineation  
162 identifiable by the relief or an offset in geological structures, which may reflect the emergence of  
163 deep-seated faults (although possibly non-seismogenic), and (2) fractured pebbles associated with a

164 fault or in the associated damage zone, which provide evidence for the seismogenic nature of the  
165 fault.

166 The first criterion is traditionally used in palaeoseismology (e.g., [Chardon et al., 2005](#); [Camelbeeck et al., 2007](#); [Baize et al., 2019](#)) and serves as a guide for trenching to study the fault's history. This  
167 approach ensures that the structures analysed in cross-section are effectively related to a deep-  
168 seated fault. The persistence of relief, however, implies that the fault has been active recently.

170 Pebble fracturing along seismogenic faults is attested by some authors, particularly [Kübler et al \(2018\)](#), in settings where the lithostatic stress is null (subsurface). Fragmentation results from the  
171 development of stress higher than pebble strength (especially in the case of poorly resistant  
172 lithologies such as argillites or sandstones) caused by shearing along the fault. This stress remains  
173 significantly lower than that required for quartz grain cataclasis (typically in deep fault gouges, e.g.,  
174 [Cashman and Cashman, 2000](#); [Torabi et al., 2007](#); [Mair and Abe, 2008](#); [Kristensen et al., 2013](#)) and  
175 requires the pebbles to be in contact with each other (clast-supported material). According to [Radjai et al. \(1998\)](#), the stress transmitted along the load-bearing network is much higher than the average  
176 vertical stress, allowing pressures higher than pebble strength to develop during shear. Seismic  
177 compression waves and waves released by the bursting of neighbouring pebbles are likely to be  
178 involved in fracturing ([Davies et al., 2012](#)), as long as fracturing is not observed along non-  
179 seismogenic faults.  
180  
181

182 Cataclasis could thus provide a reliable indicator that can be used in palaeoseismological analysis,  
183 particularly when it affects many pebbles in the damage zone around a fault ([Fig. 5A, B](#)). Other  
184 factors that can cause fracturing of subsurface pebbles include gelifraction ([Matsuoka, 2001, 2008](#);  
185 [Jia et al., 2017](#)) and mass flow of debris. Gelifraction is caused by crack expansion resulting from ice  
186 growth in fissured rocks and segregation ice growth due to water migration in weak and highly  
187 porous rocks such as chalk. Gelifraction is a common feature in cold environments and mainly affects  
188 limestones, shales and all kinds of fractured rocks ([Fig. 5C, D](#)). It remains ineffective on compact rocks  
189 such as most alluvial pebbles, for which the impacts caused by the fluvial transport have eliminated  
190 the least resistant and most fissured parts. Fractured pebbles are actually rare (but not totally  
191 absent) in Quaternary alluvial deposits and are scattered throughout the deposits. Cataclasis typifies  
192 the sedimentary flows involving a large volume of debris, i.e., rock avalanches ([Siebert, 1984](#);  
193 [Yarnold, 1993](#); [Bertran, 2003](#)). It develops within the whole flow and does not concentrate along  
194 identifiable faults. It gives rise to so-called "jigsaw" structures ([Fig. 5E, F](#)). In smaller flows (debris  
195 flows, snow avalanches), flaking of the transported blocks dominates. In most cases,



196 sedimentological criteria and the non-localized nature of cataclasis make it possible to identify the  
197 factor involved.

198 Fractured pebbles associated with faults and embedded in unconsolidated or weakly cemented  
199 fluvial deposits were mentioned by several authors ([Jorda, 1982](#); [Carbon et al., 1993](#); [Baize et al.,](#)  
200 [2002](#); [Guignard et al., 2005](#)) in southeastern France, the most seismic region of the country during  
201 historical times, and provide reliable indices for palaeo-earthquakes. To our knowledge, similar such  
202 structures have not been reported in areas further north and should focus research.

203

#### 204 Acknowledgements

205 We acknowledge O. Bellier for showing us sites with fractured pebbles in SE France. The funds have  
206 been provided by Electricité de France (EDF) and Institut de Recherches en Archéologie Préventive  
207 (Inrap) through the SISMOGEL project. M. Moretti and an anonymous reviewer are also thanked for  
208 their constructive remarks on the manuscript.

209

#### 210 References

211 [Andrieux, E., Bertran, P., Saito, K., 2016a. Spatial analysis of the French Pleistocene permafrost by a](#)  
212 [GIS database. Permafrost and Periglacial Processes 27, 17-30.](#)

213 [Andrieux, E., Bertran, P., Antoine, P., Deschodt, L., Lenoble, A., Coutard, S., 2016b. Database of](#)  
214 [pleistocene periglacial features in France: description of the online version. Quaternaire 27, 329-339.](#)

215 [Baize, S., Cushing, M., Lemeille, F., Granier, T., Grellet, B., Carbon, D., Combes, P., Hibschi, C., 2002.](#)  
216 [Inventaire des indices de rupture affectant le Quaternaire, en relation avec les grandes structures](#)  
217 [connues, en France métropolitaine et dans les régions limitrophes. Mémoires de la Société](#)  
218 [Géologique de France, Nouvelle Série, 175, 141 p.](#)

219 [Baize, S., Reicherter, K., Avagyan, A., Belyashov, A., Pestov, E., Vittori, E., Arakelyan, A., Decker, K.,](#)  
220 [2019. First assessment of recent tectonics and paleoearthquakes along the Irtysh fault \(eastern](#)  
221 [Kazakhstan\). Geomorphology 326, 90-106.](#)

222 [Ballard, J.F., Brun, J.P., Van den Driessche, J., Allemand, P., 1987. Propagation des chevauchements](#)  
223 [au-dessus des zones de décollement : modèles expérimentaux. Courier de l'Académie des Sciences](#)  
224 [de Paris 305, série II, 1249-1253.](#)

225 Bertran, P., 2003. The rock-avalanche of February 1995 at Claix (French Alps). *Geomorphology* 54,  
226 339-346.

227 Bertran, P., Andrieux, E., Bateman, M., Font, M., Manchuel, K., Sicilia, D., 2018. Features caused by  
228 ground ice growth and decay in Late Pleistocene fluvial deposits, Paris Basin, France. *Geomorphology*  
229 310, 84-101.

230 Bonini, M., 2007. Deformation patterns and structural vergence in brittle-ductile thrust wedges: An  
231 additional analogue modelling perspective. *Journal of Structural Geology* 29, 141-158.

232 Bonini, M., Sokoutis, D., Molutege, G., Katrivano, s E., 2000. Modelling hanging wall accomodation  
233 above rigid thrust ramps. *Journal of Structural Geology* 22, 1165-1179.

234 Boulton, G.S., Slot, T., Blessing, K., Glasbergen, P., Leijnse, T., van Gijssel, K., 1993. Deep circulation of  
235 groundwater in overpressured subglacial aquifers and its geological consequences. *Quaternary*  
236 *Science Reviews* 12, 739-745.

237 Brandes, C., Winsemann, J., 2013. Soft-sediment deformation structures in NW Germany caused by  
238 Late Pleistocene seismicity. *International Journal of Earth Sciences* 102, 2255-2274.

239 Branney, M.J., Gilbert, J.S., 1995. Ice-melt collapse pits and associated features in the 1991 lahar  
240 deposits of Volcan Hudson, Chile: criteria to distinguish eruption-induced glacier melt. *Bulletin of*  
241 *Volcanology* 57, 293-302.

242 Buylaert, J.P., Ghysels, G., Murray, A.S., Thomsen, K.J., Vandenberghe, D., De Corte, F., Heyse, I., Van  
243 den Haute, P., 2009. Optical dating of relict sand wedges and composite-wedge pseudomorphs in  
244 Flanders, Belgium. *Boreas* 38, 160–175.

245 Calmels, F., Allard, M., Delisle, G., 2008. Development and decay of a lithalsa in Northern Quebec: a  
246 geomorphological history. *Geomorphology* 97, 287-299.

247 Camelbeeck, T., Vanneste, K., Alexandre, P., Verbeeck, K., Petermans, T., Rosset, P., Everaerts, M.,  
248 Warnant, R., Van Camp, M., 2007. Relevance of active faulting and seismicity studies to assessments  
249 of long-term earthquake activity and maximum magnitude in intraplate northwest Europe, between  
250 the Lower Rhine Embayment and the North Sea. In: Stein, S., Mazzotti, S. (ed.), *Continental Intraplate*  
251 *Earthquakes: Science, Hazard, and Policy Issues*. The Geological Society of America Special Paper 425,  
252 pp. 193-223.

253 Carbon, D., Combes, P., Cushing, M., Granier, T., 1993. Enregistrement d'un paléoséisme dans des  
254 sédiments du pléistocène supérieur dans la vallée du Rhône : quantification de la  
255 déformation. *Géologie Alpine* 69, 33-48.

256 Cashman, S., Cashman, K., 2000. Cataclasis and deformation-band formation in unconsolidated  
257 marine terrace sand, Humbolt County, California. *Geology* 28, 111-114.

258 Chardon, D., Hermitte, D., Nguyen, F., Bellier, O., 2005. First paleoseismological constraints on the  
259 strongest earthquake in France (Provence) in the twentieth century. *Geology* 33, 901- 904.

260 Coombs, D.S., Norris, R.J., 1981. The east Abbotsford, Dunedin, New Zealand, landslide of august 8,  
261 1979, an interim report. *Bulletin de Liaison des Ponts-et-Chaussées*, n° spécial X, 27-34.

262 Coumans, J.P., Stix, J., 2016. Caldera collapse at near-ridge seamounts: an experimental investigation.  
263 *Bulletin of Volcanology* 78, 70, doi 10.1007/s00445-016-1065-9.

264 Christensen, L., 1978. Waterstress conditions in cereals used in recognizing fossil ice-wedge  
265 polygonal patterns in Denmark and northern Germany. *Proceedings of the Third International*  
266 *Conference on Permafrost*, National research Council of Canada, Edmonton, Canada, vol. 1, pp. 254-  
267 261.

268 Davison, I., Bosence, D., Alsop, G.I., Al-Aawah, M.H., 1996. Deformation and sedimentation around  
269 active Miocene salt diapirs on the Tihama Plain, northwest Yemen. In: Alsop, G.L., Blundell, D.J.,  
270 Davison, I. (eds.), *Salt tectonics*. Geological Society, London, Special Publication 100, pp. 23-39.

271 Davison, I., Alsop, G.I., Evans, N.G., Safaricz, M., 2000. Overburden deformation patterns and  
272 mechanisms of salt diaper penetration in the Central Graben, North Sea. *Marine and Petroleum*  
273 *Geology* 17, 601-618.

274 Davies, T.R.H., McSaveney, M.J., Boulton, C.J., 2012. Elastic strain energy release from fragmenting  
275 grains: effects on fault rupture. *Journal of Structural Geology* 38, 265-277.

276 Fay, H., 2000. Formation of kettle holes following a glacial outburst flood (jökulhlaup),  
277 Skeidararsandur, southern Iceland. *IAHS Publ.* 271, 205-210.

278 Geyer, A., Folch, A., Marti, J., 2006. Relationship between caldera collapse and magma chamber  
279 withdrawal: an experimental approach. *Journal of Volcanology and Geothermal Research* 157, 375-  
280 386.

281 Guignard, P., Bellier, O., Chardon, D., 2005. Géométrie et cinématique post-oligocène des failles d'Aix  
282 et de la moyenne Durance (Provence, France). *Comptes-Rendus Géoscience* 337, 375-384.

283 Guysels, G., Heyse, I., 2006. Composite-wedge pseudomorphs in Flanders, Belgium. *Permafrost and*  
284 *Periglacial Processes* 17, 145-161.

285 Hoffmann, G., Reicherter, K., 2012. Soft-sediment deformation of Late Pleistocene sediments along  
286 the southwestern coast of the Baltic Sea (NE Germany). *International Journal of Earth Sciences* 101,  
287 351-363.

288 Jia, H., Leith, K., Krautblatter, M., 2017. Path-dependent frost-wedging experiments in fractured, low-  
289 permeability granite. *Permafrost and Periglacial Processes* 28, 698-709.

290 Jorda, M., 1992. La tectonique plio-quadernaire des Préalpes de Digne et ses prolongements récents.  
291 L'enseignement des hautes nappes alluviales. In: *Le Villafranchien méditerranéen*, Université des  
292 Sciences et Techniques de Lille, 1982, 425-440.

293 Kasse, C., 1997. Cold-climate Aeolian Sand-sheet formation in North-Western Europe (c. 14-12.4 ka);  
294 a response to permafrost degradation and increased Aridity. *Permafrost and Periglacial Processes* 8,  
295 295-311.

296 Kasse, K., Bohncke, S., 1992. Weichselian Upper Pleniglacial aeolian and ice-cored morphology in the  
297 southern Netherlands (Noort-Brabant, Groote Peel). *Permafrost and Periglacial Processes* 3, 327-  
298 342.

299 Komuro, H., 1987. Experiments on cauldron formation: a polygonal cauldron and ring fractures.  
300 *Journal of Volcanology and Geothermal Research* 31, 139-149.

301 Kübler, S., Friedrich, A.M., Gold, R.D., Strecker, M.R., 2018. Historical coseismic surface deformation  
302 of fluvial gravel deposits, Schafberg fault, Lower Rhine Graben, Germany. *International Journal of*  
303 *Earth Science* 107, 571-585.

304 Kristensen, M.B., Child, C., Olesen, N.Ø., Korstgård, J.A., 2013. The microstructure and internal  
305 architecture of shear bands in sand-clay sequences. *Journal of Structural Geology* 46, 129-141.

306 Lang, J., Hampel, A., Brandes, C., Winsemann, J., 2014. Response of salt structures to ice loading:  
307 implications for ice-marginal and subglacial processes. *Quaternary Science Reviews* 101, 217-233.

308 Luzón, A., Rodríguez-López, J.P., Pérez, A., Soriano, M.A., Gil, H., Pocovi, A., 2012. Karst subsidence as  
309 a control on the accumulation and preservation of aeolian deposits: A Pleistocene example from a  
310 proglacial outwash setting, Ebro Basin, Spain. *Sedimentology* 59, 2199-2225.

311 Mackay, J.R., 1988. Pingo collapse and paleoclimatic reconstruction. *Canadian Journal of Earth*  
312 *Sciences* 25, 495-511.

313 Mackay, J.R., 1998. Pingo growth and collapse, Tuktoyaktuk Peninsula area, western Arctic coast,  
314 Canada: A long-term field study. *Géographie Physique et Quaternaire* 52, 271-323.

315 Mair, K., Abe, S., 2008. 3D numerical simulations of fault gouge evolution during shear: Grain size  
316 reduction and strain localization. *Earth and Planetary Science Letters* 274, 72-81.

317 Marco, S., Weinberger, R., Agnon, A., 2002. Radial clastic dykes formed by a salt diapir in the Dead  
318 Sea Rift, Israel. *Terra Nova* 14, 288-294.

319 Matsuoka, N., 2001. Microgelivation versus macrogelivation: towards bridging the gap between  
320 laboratory and field frost weathering. *Permafrost and Periglacial Processes* 12, 299-313.

321 Matsuoka, N., 2008. Frost weathering and rockwall erosion in the southeastern Swiss Alps: Long-term  
322 (1994–2006) observations. *Geomorphology* 99, 353-368.

323 McCalpin, J.P., Thakkar, M.G., 2003. 2001 Bhuj-Kachchh earthquake: surface faulting and its relation  
324 with neotectonics and regional structures, Gujarat, Western India. *Annals of Geophysics* 46, 937-956.

325 McDonald, B.C., Shilts, W.W., 1975. Interpretation of faults in glaciofluvial sediments. In: Jopling,  
326 A.V., McDonald, B.C. (eds.), *Glaciofluvial and glaciolacustrine sedimentation*. Society of Economic  
327 Paleontologists and Mineralogists, Tulsa, USA, Special Publication 23, pp. 123-131.

328 Moretti, M., Alfaro, P., Owen, G., 2016. The environmental significance of soft-sediment deformation  
329 structures: key signatures for sedimentary and tectonic processes. *Sedimentary Geology* 344, 1-4.

330 Murton, J.B., 1996. Thermokarst-lake-basin sediments, Tuktoyaktuk Coastlands, western arctic  
331 Canada. *Sedimentology* 43, 737-760.

332 Murton, J.B., 2005. Ground-ice stratigraphy and formation at North Head, Tuktoyaktuk Coastlands,  
333 Western Arctic Canada: a product of glacier–permafrost interactions. *Permafrost and Periglacial*  
334 *Processes* 16, 31-50.

335 Murton, J.B., 2013. Ice wedges and ice wedge casts. In: Elias, S.A., Mock, C.J. (Eds.), *Encyclopedia of*  
336 *Quaternary Science*. Elsevier, Amsterdam, pp. 436-451.

337 Payette, S., Séguin, M.K., 1979. Les buttes minérales cryogènes dans les basses terres de la Rivière-  
338 aux-Feuilles, Nouveau Québec. *Géographie Physique et Quaternaire* XXIII, 339-358.

339 Philip, H., Rogozhin, E., Cisternas, A., Bousquet, J.C., Borisov, B., Karakhanian, A., 1992. The Armenian  
340 earthquake of 1988 December 7: faulting and folding, neotectonics and palaeoseismicity.  
341 *Geophysical Journal International* 110, 141-158.

342 Pissart, A., 2000. Remnants of lithalsas of the Hautes Fagnes, Belgium: a summary of present-day  
343 knowledge. *Permafrost and Periglacial Processes* 11, 327–355.

344 Pollard, W.H., 1991. Seasonal frost-mounds. *The Canadian Geographer* 35, 2014-2018.

345 Radjai, F., Wolf, D.E., Jean, M., Moreau, J.J., 1998. Bimodal Character of Stress Transmission in  
346 Granular Packings. *Physical Review Letters* 80, 61-64.

347 Ravier, E., Buoncristiani, J.F., Menzies, J., Guiraud, M., Portier, E., 2015. Clastic injection dynamics  
348 during ice front oscillations: a case example from Sólheimajökull (Iceland). *Sedimentary Geology* 323,  
349 92–109.

350 Roche, O., van Wyk de Vries, B., Druitt, T.H., 2001. Sub-surface structures and collapse mechanisms  
351 of summit pit. *Journal of Volcanology and Geothermal Research* 105, 1-18.

352 Sanford, A.R., 1959. Analytical and experimental study of simple geologic structures. *Bulletin of the*  
353 *Geological Society of America* 70, 19-52.

354 Siebert, L., 1984. Large volcanic debris avalanches: characteristics of source areas, deposits, and  
355 associated eruptions. *Journal of Volcanology and Geothermal Research* 22, 163–197.

356 Simón, J.L., Soriano, A., 1986. Diapiric deformations in the Quaternary deposits of the central Ebro  
357 Basin, Spain. *Geological Magazine* 123, 45-57.

358 Simón, J.L., Soriano, M.A., Pérez, A., Luzón, A., Pocovi, A., Gil H., 2014. Interacting tectonic faulting,  
359 karst subsidence, diapirism and continental sedimentation in Pleistocene deposits of the central Ebro  
360 Basin (Spain). *Geological Magazine* 151, 1115-1134.

361 Soriano, M.A., Luzón, A., Yuste, A., Pocovi, A., Pérez, A., Simón, J.L., Gil H., 2012. Quaternary alluvial  
362 sinkholes: record of environmental conditions of karst development, examples from the Ebro Basin,  
363 Spain. *Journal of Cave and Karst Studies* 74, 173-185.

364 Torabi, A., Braathen, A., Cuisiat, F., Fossen, H., 2007. Shear zones in porous sand: insights from ring-  
365 shear experiments and naturally deformed sandstones. *Tectonophysics* 437, 37-50.

366 Vandenberghe, J., French, H., Gorbunov, A., Marchenko, S., Velichko, A.A., Jin, H., Cui, Z., Zhang, T.,  
367 Wan, X., 2014. The Last permafrost Maximum (LPM) map of the Northern Hemisphere: permafrost  
368 extent and mean annual air temperatures, 25-17 ka. *Boreas* 43, 652-666.

369 Van Loon, A.J., Pisarska-Jamrozy, M., 2014. Sedimentological evidence of Pleistocene earthquakes in  
370 NW Poland induced by glacio-isostatic rebound. *Sedimentary Geology* 300, 1-10.

371 Van Loon, A.J., Pisarska-Jamrozy, M., Nartiss, M., Krievans, M., Soms, J., 2016. Seismites resulting  
372 from high-frequency, high-magnitude earthquakes in Latvia caused by Late Glacial glacio-isostatic  
373 uplift. *Journal of Palaeogeography* 5, 360-380.

374 [Walter, T.R., Troll, V.R., 2001. Formation of caldera periphery faults: an experimental study. Bulletin](#)  
375 [of Volcanology 63, 191-203.](#)

376 [Yarnold, J.C., 1993. Rock-avalanche characteristics in dry climates and the effect of flow into lakes:](#)  
377 [insights from mid-Tertiary sedimentary breccias near Artillery Peak, Arizona. Geological Society of](#)  
378 [America Bulletin 105, 345– 360.](#)

379 [Zeeberg, J., 1998. The European sand belt in Eastern Europe and comparison of Late Glacial dune](#)  
380 [orientation with GCM simulation results. Boreas 27, 127–139.](#)

381

382 Figure captions

383 Figure 1. (A) Pleistocene sand wedge, Salaunes (SW France), (B) Close up view of the vertical  
384 lamination in a sand wedge from La Louverie (Loire valley, France), (C) Sand wedge with apophyses,  
385 Saint-Amand-les-Eaux (N France), (D) Globular structure (DSW) caused by the deformation of a sand  
386 wedge, Saint-André-de-Cubzac (SW France); the sand wedge (SW) is visible on the bottom of the  
387 trench below the dotted line.

388 Figure 2. (A) Ground thermal contraction polygons, Peissen (X = 9.5878°E, Y = 54.0414°N); (B)  
389 Polygons, Beldorf (X = 9.3540°E, Y = 54.1213°N) (Google Earth, photos 2009).

390 Figure 3. Brittle deformation of sandy soil models. (A) Radial fractures and central polygonal  
391 depression formed by the rise of a ball under a granular cover, redrawn from Komuro (1987); (B)  
392 Fracturing of a sand cover following chamber inflation, from Walter and Troll (2001); (C) Formation of  
393 curved reverse faults in sand due to the lifting of a substratum block, from Sanford (1959); (D) Bell-  
394 shaped reverse faults above a cavity, from Geyer et al. (2006); (E) Annular fracture above a cavity,  
395 from Walter and Troll (2001) (the chamber is indicated by the grey dashed line); (F) Deformation  
396 after swelling followed by emptying of a chamber, from Walter and Troll (2001); (G) Asymmetric  
397 collapse above a cavity in the presence of a relief, from Coumans and Stix (2016); (H) Deformation of  
398 a cover as a result of horizontal shortening, from Ballard et al. (1987).

399 Figure 4. (A) Radial cracks on a pingo (ice-cored mound), Tuktoyaktuk, Canada (Google Earth); (B)  
400 Radial and tangential faults around a salt diapir, redrawn from Davison et al. (2000); (C) Reverse  
401 faults in Pleistocene thermokarst lake deposits, Gourgançon (Paris Basin, France); (D) Thrust planes  
402 at the toe of a landslide, Les Leches (SW France); (E) Bell-shaped reverse faults above a karstic cavity,  
403 Mérégnac (SW France).

404 Figure 5. (A, B) Fractured pebbles in the Lower Pleistocene Valensole II Formation, near Sisteron (SE  
405 France); the finer-grained material to the left of photo B is a fault gouge; the largest pebble is 10 cm  
406 long; (C) Gelifracted pebble in an active layer above permafrost, Tuktoyaktuk (Canada); (D)  
407 Gelifracted sandy limestones, French Pyrenees (France); the largest pebbles are 20 cm in diameter;  
408 (E) Jigsaw structure in the Mont Granier rock avalanche (French Alps); knife for scale; (F) Jigsaw  
409 structure in a volcanic rock avalanche, Guadeloupe Island (French West Indies); the section is 1.5 m  
410 high.



Figure (Color)  
[Click here to download high resolution image](#)

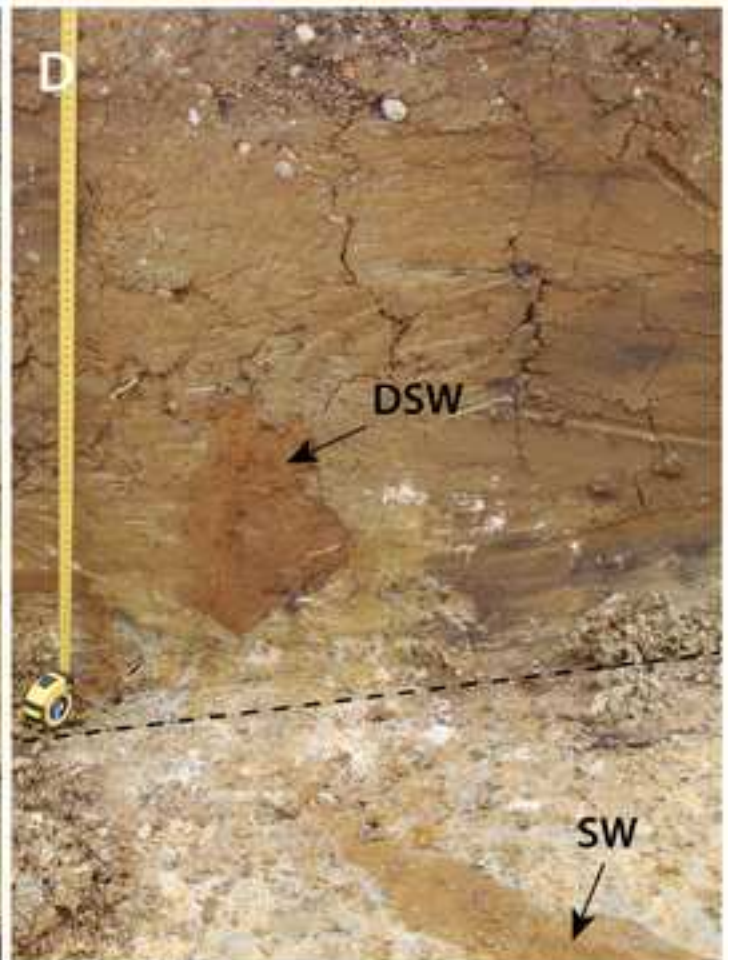


Figure (Color)  
[Click here to download high resolution image](#)



Figure (Color)  
[Click here to download high resolution image](#)

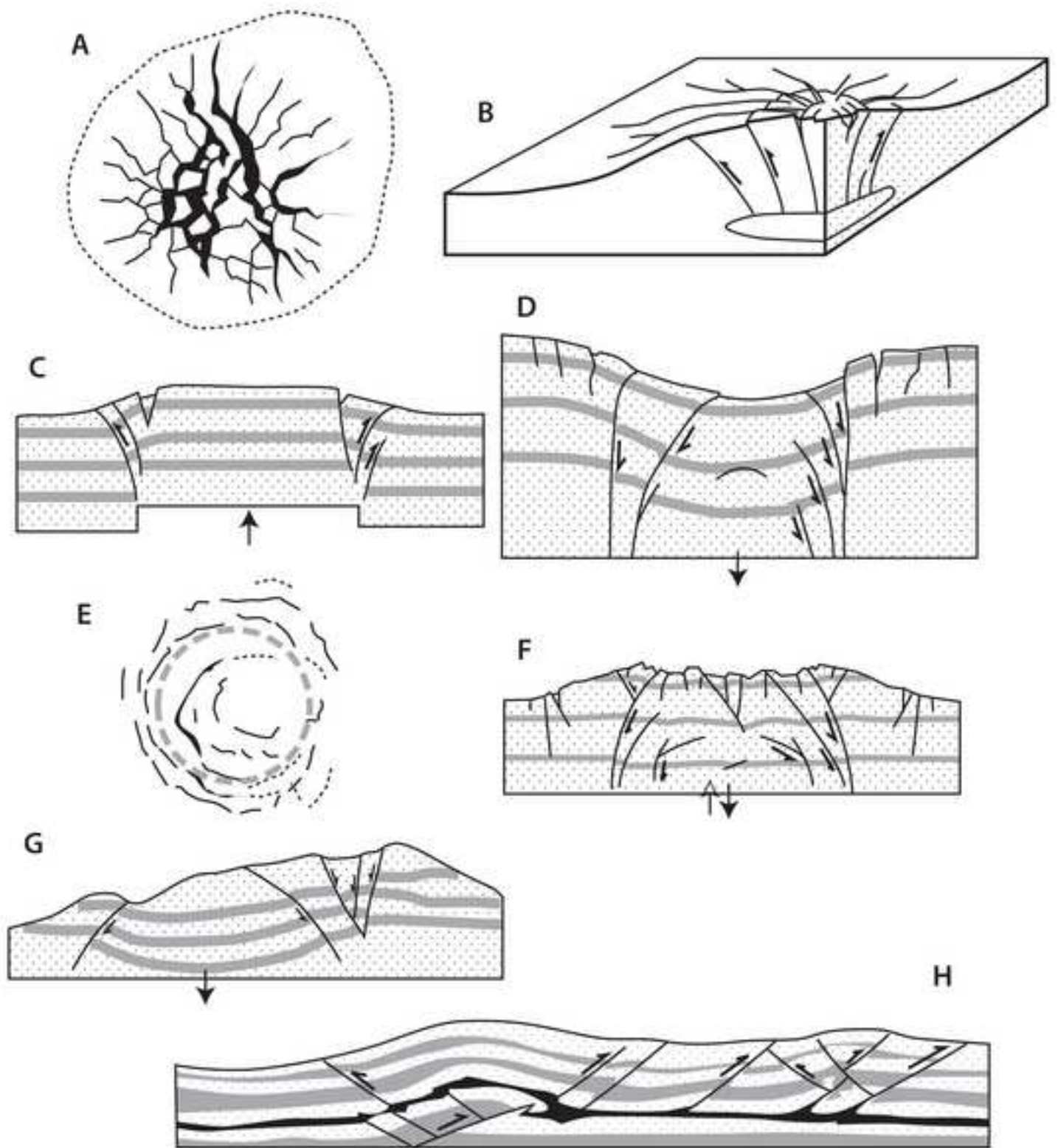


Figure (Color)  
[Click here to download high resolution image](#)

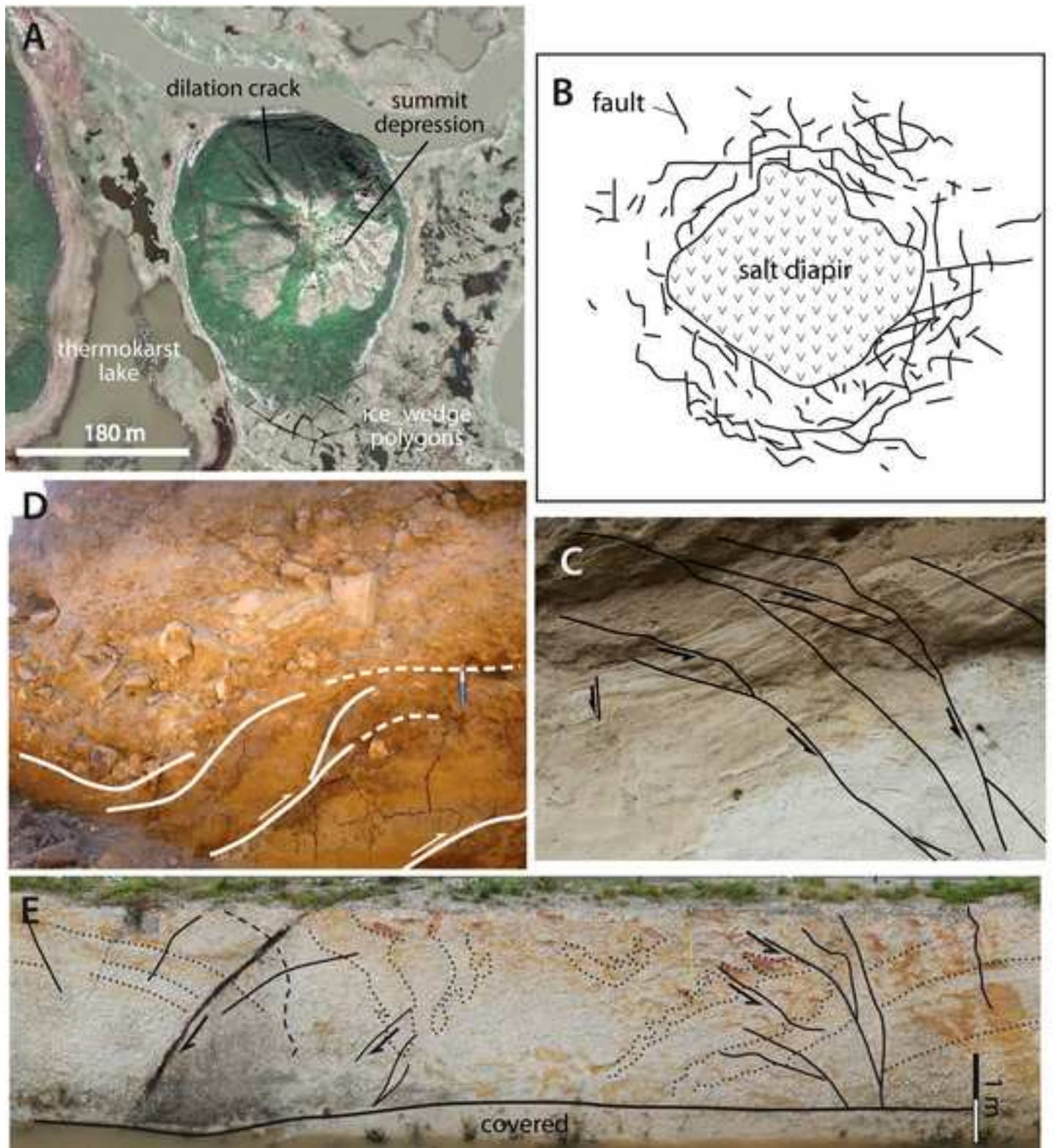


Figure (Color)  
[Click here to download high resolution image](#)

